Supplementary Materials for

Live imaging of neurogenesis in the adult mouse hippocampus

Gregor-Alexander Pilz, Sara Bottes, Marion Betizeau, David J. Jörg, Stefano Carta, Benjamin D. Simons, Fritjof Helmchen, Sebastian Jessberger

Correspondence to: jessberger@hifo.uzh.ch

This PDF file includes:

Other Supplementary Materials for this manuscript includes the following:

1 Materials and Methods

Experimental animals and sparse labeling of NSPCs

All experimental procedures were conducted in accordance with the ethical principles and guidelines for animal experiments of the Veterinary Office of Switzerland and were approved by the Cantonal Veterinary Office in Zurich.

Ascl1Cre ERT2 mice (*Ascl1*$^{tm1.1(Cre/ERT2)Jejo}$; JacksonLab strain 012882) crossed to the CAG tdTomato (Ai14; B6.Cg-*Gt(ROSA)*$^{26Sortm14(CAG-tdTomato)Hze}$; JacksonLab strain 007914) reporter strain were used for the entire study. Mice aged 6–7 weeks were used for hippocampal window implantation. For labeling a sparse population of NSPCs, a single dose of Tamoxifen (70–80mg/kg in corn oil; Sigma) was injected intraperitoneally 2 weeks after implantation of the hippocampal window. We aimed to label 10–20 SPOTs (SPOT is an imaging field of view that contains labeled tdTomato positive cells) containing single labeled R cells in the dorsal dentate gyrus (DG).

Implantation of a chronic hippocampal window

A transcortical hippocampal window was implanted in mice aged 6-7 weeks as described before [21]. In brief, after opening of the skin the cranial bone above the hippocampus (–2.0 posterior /–1.7 lateral mm from Bregma) was removed using a dental drill. Thereafter a biopsy-punch (3 mm diameter; Miltex) was inserted in a defined depth (1.5 mm). Using a blunt 22-gauge needle connected to a pump the cortical tissue was carefully aspirated until the white matter fibers of the corpus callosum become visible. After the bleeding has stopped, the hippocampal window, consisting of a stainless steel cannula (height: 1.5 mm; OD: 2.7 mm, ID: 2.5 mm) and a coverglass (3 mm diameter; Warner instruments) was inserted into the opening, kept in place using a micromanipulator, and glued to the skull using UV curable dental glue (Ivoclar Vivadent).

In vivo imaging in the DG

Imaging was started 2 days after Tamoxifen injection ($>$ 2 weeks after window implantation). An aluminum head post was glued onto the contralateral side of the cranial bone using UV curable dental cement (Ivoclar Vivadent) to stably secure the animals head in a frame during imaging. Mice were anesthetized under the microscope using isoflurane (1.5–2% in O_2) while the body temperature was constantly monitored and regulated at 37°C with a heating pad. In addition the breathing rate was monitored frequently. We used a custom-built, two-photon microscope of the Sutter Instrument Movable Objective Microscope type, equipped with a 16x long-working-distance, water-immersion objective (0.8 NA, Nikon), a Pockels cell (model 350/80 with controller model 302RM, Conoptics), and galvanometric scan mirrors (model 6210, Cambridge Technology)[21], controlled by the HelioScan software [39]. For excitation of tdTomato, we used a ytterbium-doped potassium gadolinium tungstate (Yb:KGW) laser at 1040 nm (Time Bandwidth Products). Fluorescence was collected through a red emission filter (610/75 nm; AHF Analysetechnik) and detected with a photomultiplier tube (Hamamatsu). Ringer's solution (containing (in mM) 135 NaCl, 5.4 KCl, 5 HEPES, 1.8 CaCl2, pH 7.2) was used as immersion medium. One rim of the cannula was used as a landmark to set the zero position ($x = 0$, $y = 0$, $z = 0$). A map with coordinates of the individual SPOTs containing NSPCs was noted down and used to relocate the SPOTs in the fol-

lowing imaging sessions. Each SPOT was imaged in a repetitive manner (shortest interval 12 hrs) taking a z-stack (5 μm stepsize, averaging 3 x) with 2x zoom that included all cells of the clone. The average laser power measured beneath the objective for exciting tdTomato was 202 mW. Due to scattering in the tissue at 600 - 800 μm depth, we estimate the laser power in the focal volume to be more than 10 - 40 times lower, taking into account a scattering length of 200 - 250 μm at 920 - 1040nm [40]. The signal strength of tdTomato increases rapidly after induction so the laser power could be progressively reduced. The imaging per mouse was limited to maximally one hour. SPOTs were revisited in each imaging session and checked for changes. If no changes occurred, this was noted and no z-stack was taken.

Post-imaging immunohistochemistry and confocal microscopy

During deep anesthesia (Burprenophine) animals were perfused first with cold saline and then paraformaldehyde (4% in phosphate buffer). The brain was dissected out leaving the hippocampal window in place for overnight post fixation. After dehydration for minimum 2 days in sucrose (30% in PBS) sections were cut at 60 μm thickness in horizontal orientation (corresponding to the view during imaging) on a cryotom (Leica SM2010R). Sections were stained for Sox2 (1:500, goat, SantaCruz), Nestin (1:500, mouse, BD), Prox1 (1:500, rabbit, Millipore), GFAP (1:500, mouse, Sigma), Tbr2 (1:200, rabbit, Abcam), Ki67 (1:250, rabbit, Abcam), Olig2 (1:250, rabbit, Millipore) BrdU (1:200, rat, Abcam). To stain for BrdU, sections were pretreated with 2N HCl (37°C) for 30 min followed by treatment with 0.1M borate buffer (pH 8.8) for 10 min at room temperature. Pictures of stained sections were taken with a confocal laser-scanning microscope (Olympus FV1000). For the quantification of recombined cells per area (Figure S1I) the DAPI dense area of the granule cell layer (maximum projection of first six horizontal sections that contained DG; sections were 60μm thick) was outlined and measured using FIJI [41].

Image processing and coding of imaging data

The first analysis of the raw data was carried out using FIJI [41]. All imaging time points of a SPOT were compiled into a single image stack that allowed access to all z-stacks at all time points. Going through each z-level at each time point cells were carefully analyzed and categorized. Importantly the dynamic behavior of cells (morphology changes, migration, division) was taken into account in order to identify the cell type and also lineage relationships (e.g. location of cells in relation to all surrounding cells). All z-planes of a stack were analyzed in order to identify the potential presence of radial processes (Movie S1, S2). Depending on the orientations of R cells within the granule cell layer, radial processes may not be readily visible in the maximum projection of a stack, but become evident when all individual z-planes are analyzed. In addition, the information of all z-planes was used to distinguish neighbouring cell bodies during the expansion of clones (Movie S2). R cell annotation was also based on the inheritance of a basal process, whereas NR cells only extend shorter and less stable processes, as judged by analyzing z-planes at subsequent time points. Using the ROI manager in FIJI each individual cell of a clone received a code. See Table S1 for detailed code explanation.

Each NSPC lineage was annotated by an individual researcher and cross-checked by a blinded second researcher. In the case that both experimenters considered a cell type or lineage transition uncertain, this was saved as such. This code for all cells appearing in the lineage could be reloaded

to check and re-identify cells at any time. After generation of an annotated lineage tree (each indicated cell is depicted with its cell ID and time point) the original raw data file (Image 5D) and ROI set is revisited to clarify the judgment of cell types and lineage transitions.

3D reconstruction of R cells were obtained using the fill function from the Simple Neuron Tracer plugin [42], 3D visualization of the fills were performed with ImageJ 3D viewer [43]. Movie editing was carried out in Premiere Pro (Adobe).

Data analysis in R

The compilation of the tree annotations and subsequent data analysis / statistics was performed in R software [44] using custom made scripts. Unless specified differently in the figure legend, data are presented as mean $\pm$ s.e.m. For every lineage, a text file containing the code as well as the x, y, z coordinates and the time point of every cell on every image was extracted using FIJI. All the different exported files were compiled into one full dataset, where every part of the code was translated into a different column. The dataset consists of 63 lineages recorded on 9 different animals with on average 7 ± 2.3 clones per animal for a total of 916 cells and 853 lineage transitions. In the subsequent data analysis, if a cell was observed for longer than 7 days without dividing (95th percentile of NR cell cycles) and showed neurite extension it was considered as neuron (see Table S1).

871 out of 916 cell types (95%) could be identified with certainty. 491 out of 853 lineage transitions (58%) could be mapped unambiguously. For every analysis where the cell type or lineage information is used, only cells for which these parameters could be unambiguously identified are considered.

The Div of each cell refers to the generation the cell is born in. The root cell of the tree is set to Div1, its daughter cells are at Div2 and so forth. We also defined the NR Div for NR cells where Div1 is set at the first NR cell arising in the branch of the tree.

The cell division time (T_D) was computed as the duration between two successive divisions. Due to the low temporal resolution of the recordings, a minimum and a maximum T_D was computed, the mean of these two values is displayed. If the cumulated uncertainty in the timing of the two successive divisions was higher than 6 days the T_D value was not considered.

The cell death rate per lineage is defined as the percentage of dying terminal cells over the total number of terminal cells in each tree. For the death rate in subtrees analysis, subtrees were considered only if the main tree generated at least 4 terminal cells, and exactly 2 subtrees. To account for asymmetrical sublineages, the standard deviation of death rates at a given Div was weighted by the number of cells in the progeny of each sublineage. The wtd.stats function of Hmisc package was used [45].

The tree visualization was performed using the igraph package of R [46]. Lattice, pheatmap, and ggplot2 packages were used for data visualization [47–49].

Morphometric index analysis (MMI)

Images were acquired as z-stacks from the 2-photon microscope setup (view previous section). Z-stacks were first collapsed into a maximum intensity projection (MIP) followed by adjustment of brightness and contrast (as well as inversion of LUT) in Fiji image software and manually drawing

an outline in GIMP2 (v.2.8) with the help of simultaneous consideration of each z-plane in the original z-stack [41]. This strategy allowed to carefully distinguish mother from daughter cells and additionally clarify overall morphological features. Outlines from collapsed z-stacks were then reimported into Fiji image software where circularity $= (4\pi \cdot \frac{\text{Area}}{\text{Perimeter}^2})$ as well as apical process length were measured in pixels. To quantify morphological changes of R cells before and after division, we defined a morphological index, which reflects both changes in the shape of the soma via its circularity (formula), and change in its degree of polarity via the length of its apical process. A perfectly circular R cell will have a value of 1, with progressively lower values as the soma becomes ellipsoid and increases relative to area [50]. Apical process length was measured from edge of the cell body following the process towards the first bifurcation (or in case of no bifurcation until the end of the process). The product of these two parameters, which we called morphometric index (MMI), was calculated for each R cell before (t_0) and after (t_1) an asymmetric division. ΔMMI was determined as the relative difference between these 2 time points with t0 as reference.

Statistical analysis

The statistical analysis of the data was performed using the R software [44]. Performed tests and corresponding p-values are indicated in the figure legend. For data involving proportions of small number of data points, the Fischer's exact test was used. When data did not follow a normal distribution according to the Shapiro-Wilk test, non-parametric tests were preferred. Wilcoxon test was performed for mean comparison, Kruskal-Wallis test for one-way ANOVA. Alternatively, an unpaired two way t-test was used for mean comparison.

Theoretical model

In our theoretical framework, the state of a clone is given by a population of cells $i = 1, \ldots, n(t)$ together with the elapsed time t_i since their last division or birth. Cell types are radial glia-like cells (R), non-radial progenitors (NR) and neurons (N). When a cell undergoes a cell fate event, it is either chosen to die (with a cell-type specific probability ω) or to divide (with probability $1-\omega$). R cells undergo a deterministic cell fate program consisting of r_1 symmetric self-renewing divisions (SR), followed by r_2 asymmetric divisions (A) during which they give rise to one NR cell per division, followed by a differentiating symmetric division (SD) (Fig. S6A). NR cells follow a purely stochastic cell fate behavior, choosing between SR, SD, and A with probabilities p_{NR}, q_{NR} and $1 - p_{\text{NR}} - q_{\text{NR}}$, respectively (Fig. S6C). N cells can only undergo cell death (Fig. S6D).

Cells undergo these cell fate events in stochastically determined time intervals to reflect their cycle time distribution. A successful strategy to capture long-term clonal dynamics has been to represent cell fate processes by Markovian birth-death processes [51–53], an approach which entails exponentially distributed cell cycle times. Since we here consider the short-time cell fate dynamics (i.e., a few rounds of cell division), details of the cell cycle time distribution become important. Therefore, we here represent cell fate events by non-Markovian processes reflecting the experimentally determined (non-exponential) cell cycle time distributions. To compute the order of and the time intervals between fate events, we employ a non-Markovian stochastic simulation framework [54], which requires to specify a cell-type specific waiting time distribution $\psi_i(\tau)$ for each cell i. For details on the algorithm, we refer the reader to Ref. [54].

Empirically, experimentally obtained persistence time distributions (time until next division or death) conform well to distributions of the Fréchet type, which we use as waiting time distributions, $\psi_i(\tau) = F_{\mu_i \nu_i}(\tau)$, with

$$F_{\mu\nu}(\tau) = \mu \nu^{\mu} \tau^{-\mu-1} \mathrm{e}^{-(\nu/\tau)^{\mu}} , \qquad (\tau \geq 0) . \tag{S1}$$

For each cell type, we determine the set of shape parameters (μ, ν) by pooling the recorded persistence times into bins with a time intervals $\Delta\tau = 1\,\mathrm{d}$ and fitting the bin probabilites $f_{\mu\nu,k} = \int_{k\,\Delta\tau}^{(k+1)\,\Delta\tau} F_{\mu\nu}(\tau)\,\mathrm{d}\tau$ using a standard least-squares approach (Fig. S7A).

Each simulated lineage tree starts with a single R cell with zero elapsed time and is simulated for a specified total duration T_{sim}. We take into account the unknown uncertainty about the generation of the initially marked cell as follows: Once the simulation terminates, a random generation g between 1 and G is determined where G is the uncertainty in the initial generation. Among all cells of generation g, one is selected randomly and only this cell and its entire subtree are kept. Subsequently, the global time is shifted so that the new apex of the lineage tree has time zero. Only cell fate events within a specified observation time window T_{obs} are kept. From the set of $N = 55$ experimentally obtained lineage trees with active R cells, we retrieve their observation durations $T_{\mathrm{obs},1}, \ldots, T_{\mathrm{obs},N}$ and simulate N lineage trees. Each lineage tree $l = 1, \ldots, N$ is simulated for a multiple of the observation time, $T_{\mathrm{sim},l} \gg T_{\mathrm{obs},l}$, so that after determining the initial generation and truncating, the simulated lineage tree has the same length $T_{\mathrm{obs},l}$ as the corresponding experimental lineage tree. This ensures that the effects of lineage tree truncation by finite experimental observation times is accounted for in our model. To obtain statistics on the simulated lineage trees, we repeat this procedure M times, so that we simulate a total ensemble of $M \times N$ lineage trees (see Supplementary Table S2).

The parameters ω_{R}, ω_{NR}, p_{NR}, and q_{NR} are determined by their relative frequency among all cell fate events in all experimental lineage trees for the respective cell type. To obtain fits for the remaining parameters r_1, r_2, ω_{N}, and G, we apply the following procedure. From experimental data, we obtain the number of newborn cells and the time-dependent cell fate frequencies for successive time intervals of 5 days. For each interval k, we determine (i) the number $m_{x,k}$ of newborn cells in the time interval for the different cell types x and (ii) the cell fate probabilites $P_{x,\eta,k}$, i.e., the relative frequencies of different cell fates occurring during the time interval for different cell types $x = \mathrm{R}, \mathrm{NR}, \mathrm{N}$, where η indicates the division mode (SR, A, SD) or death (D). Based on these observables, we define the residuals between theoretical and experimental results as $R_m = \sum_{x=1}^{3} \sum_k (m_{x,k}^{\mathrm{exp}} - m_{x,k}^{\mathrm{th}})^2$ and $R_P = \sum_\eta \sum_k (P_{\mathrm{R},\eta,k}^{\mathrm{exp}} - P_{\mathrm{R},\eta,k}^{\mathrm{th}})^2$. Computing the residuals for each simulated parameter set, we give each set two ranks ϱ_m and ϱ_P based on their residuals R_m and R_P. The best fit is defined as the parameter set with the highest (i.e., smallest) combined rank $\varrho_m + \varrho_P$. The parameter ω_{N} is determined by fitting the number of neurons per clone averaged over all clones and times. For the fits, simulation averages are taken over $M = 100$ realizations of all $N = 55$ lineage trees, i.e., from 5500 simulated lineage trees per parameter set. The best parameter fit values are reported in Supplementary Table S2. A comparison of the results of the fit with the experimental data on the number of newborn cells per time interval, the time-dependent cell fate frequencies, and the average clone content are shown in Fig. S7B–D.

Statistical test for stochastic fate decisions

To test whether the observed pattern might be a chance outcome of a stochastic fate behavior with time-shifting probabilities, we adapt the theoretical model as follows (abbreviating the original model by M and the altered model by M'). We replace the fate behavior of R cells by the following rule: Upon each cell division, R cells choose stochastically between SR, SD, and A divisions with time-dependent probabilities $p_1(t), q_1(t)$, or $1 - p_1(t) - q_1(t)$, respectively (Fig. S6B). The time-dependence of the probabilities p_1 and q_1 is given by $p_1(t) = \max(c_p - \kappa_p t, 0)$ and $q_1(t) = \min(c_q + \kappa_q t, 1)$, where c_p and c_q are the probabilites at the time of induction ($t = 0$) and κ_p and κ_q are the rates with which the probabilities linearly change in time. All other rules of the model remain unchanged. The parameters c_p, c_q, κ_p and κ_q are directly determined from linear fits of the relative frequencies of the respective cell fate events obtained from experimentally recorded lineage trees, see Fig. S7E. All remaining parameters are determined using the same fit strategy as the original model. To probability to never observe an R cell division pattern involving at least one SR division following another SR or a A division under the model hypothesis M' was computed as follows. We simulated all 55 lineage trees 500 times using the optimal fit parameters indicated in Supplementary Table S2 and obtained 12 resulting tree sets in which it was the case, resulting in a probability of $2.4\,\%$.

References

[39] D. Langer, M. van't Hoff, A. J. Keller, C. Nagaraja, O. A. Pfäffli, M. Göldi, H. Kasper, and F. Helmchen. Helioscan: A software framework for controlling in vivo microscopy setups with high hardware flexibility, functional diversity and extendibility. *J. Neurosci. Methods*, 215(1):38–52, 2013.

[40] D. Kobat, M. E. Durst, N. Nishimura, A. W. Wong, C. B. Schaffer, and C. Xu. Deep tissue multiphoton microscopy using longer wavelength excitation. *Optics Express*, 17(16):13354–13364, 2009.

[41] J. Schindelin, I. Arganda-Carreras, E. Frise, V. Kaynig, M. Longair, T. Pietzsch, S. Preibisch, C. Rueden, S. Saalfeld, B. Schmid, J.-Y. Tinevez, D. J. White, V. Hartenstein, K. Eliceiri, P. Tomancak, and A. Cardona. Fiji: an open-source platform for biological-image analysis. *Nat. Methods*, 9(7):676–682, 2012.

[42] M. H. Longair, D. A. Baker, and J. D. Armstrong. Simple neurite tracer: open source software for reconstruction, visualization and analysis of neuronal processes. *Bioinformatics*, 27(17):2453–2454, 2011.

[43] B. Schmid, J. Schindelin, A. Cardona, M. Longair, and M. Heisenberg. A high-level 3d visualization API for java and ImageJ. *BMC Bioinformatics*, 11(1):274, 2010.

[44] R Core Team. *R: A Language and Environment for Statistical Computing*. R Foundation for Statistical Computing, Vienna, Austria, 2017.

[45] F. E. Harrell. Hmisc: Harrell miscellaneous. R package version 4.0-1, 2016.

[46] G. Csardi and T. Nepusz. The igraph software package for complex network research. InterJournal, Complex Systems, 2006.

[47] D. Sarkar. *Lattice: Multivariate Data Visualization with R*. Springer-Verlag New York, 2008.

[48] H. Wickham. *ggplot2: Elegant Graphics for Data Analysis*. Springer-Verlag New York, 2009.

[49] R. Kolde. pheatmap: Pretty Heatmaps. R package version 1.0.8, 2015.

[50] D. Chitsaz, D. Morales, C. Law, and A. Kania. An Automated Strategy for Unbiased Morphometric Analyses and Classifications of Growth Cones In Vitro. *PLOS ONE*, 10(10):1–21, 10 2015.

[51] E. Clayton, D. P. Doupé, A. M. Klein, D. J. Winton, B. D. Simons, and P. H. Jones. A single type of progenitor cell maintains normal epidermis. *Nature*, 446:185–189, 2007.

[52] A. M. Klein, T. Nakagawa, R. Ichikawa, S. Yoshida, and B. D. S. Mouse germ line stem cells undergo rapid and stochastic turnover. *Cell Stem Cell*, 7(2):214–224, 2010.

[53] A. Sánchez-Danés, É. Hannezo, J.-C. Larsimont, M. Liagre, K. K. Youssef, B. D. Simons, and C. Blanpain. Defining the clonal dynamics leading to mouse skin tumour initiation. *Nature*, 536(7616):1–22, 2016.

[54] M. Boguñá, L. F. Lafuerza, R. Toral, and M. Ángeles Serrano. Simulating non-Markovian stochastic processes. *Phys. Rev. E*, 90(4):042108, 2014.

2 Supplementary Figures

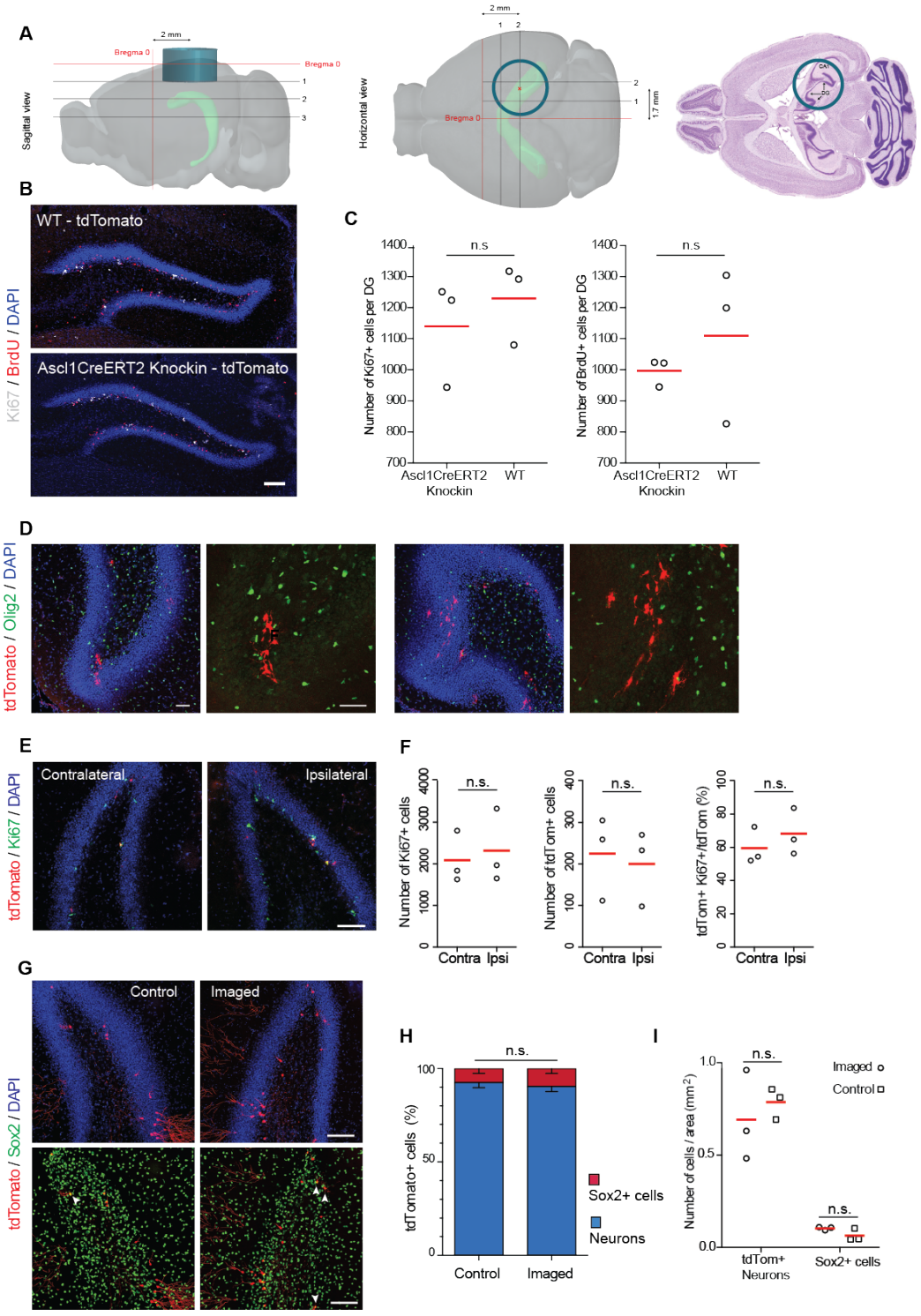

Figure S1. Hippocampal window implantation does not affect Tam-induced recombination, NSPC proliferation, and neuronal output of Ascl1-labeled cells. **(A)** Schematic representations of the placement of the transcortical hippocampal window in sagittal and horizontal views.

The position (center of the 3mm diameter circle) is -2.0 mm posterior / -1.7 mm lateral from Bregma. **(B)** Comparison of cell proliferation by staining for Ki67 (gray) and BrdU (red) in WT and Ascl1CreERT2 knockin mice at 7 weeks of age. **(C)** Quantification of proliferation by Ki67 (Ascl1CreERT2 knockin: 1140 $\pm$ 98.1; WT littermates: 1230 $\pm$ 75.2; $p = 0.509$) and BrdU stainings (Ascl1CreERT2 knockin: 997 $\pm$ 26.0; WT littermates: 1110 $\pm$ 145.0; $p = 0.520$) reveals no significant difference between Ascl1CreERT2 knockin mice and WT littermates. Statistical test used: unpaired two tailed t-test. $n = 3$; red line: mean. **(D)** No oligodendrocyte precursor cells (Olig2+; green) are recombined in the Ascl1CreERT2 tdTomato mouse at 6dpi ($n = 291 cells$). **(E)** Immunostained images (single z-stack) of contralateral and ipsilateral sides of the DG depicting Ki67+ cells (green), Ascl1-tdTomato+ cells (red) 2dpi and 2 weeks post window implantation. **(F)** The dot plots show no significant difference in proliferation (Ki67+ cell; contralateral side: 2087 $\pm$ 358.9; ipsilateral side: 2315 $\pm$ 514; $p = 0.736$), number of recombined cells (Ascl1-tdTomato+ cells; contralateral side: 225 $\pm$ 58.2; ipsilateral side: 200 $\pm$ 52.2; $p = 0.765$) and in the percentage of Ki67+/Ascl1-tdTomato+ over Ascl1-tdTomato+ cells (contralateral side: 59.62 $\pm$ 6.38; ipsilateral side: 68.26 $\pm$ 8.08; $p = 0.451$) between the two sides. Statistical test used: unpaired two tailed t-test. $n = 3$; red line: mean. **(G)** Immunostained images of control (age-matched mice without window) and imaged DG depicting Sox2+ cells (green), Ascl1-tdTomato+ cells (red) 2 month post induction (mpi). Control animals received identical Tam treatment. Arrowheads indicate tdTomato+/Sox2+ cells; tdTomato+/Sox2- cells are neurons (identified by morphology). **(H)** Bar graph shows no significant differences in the percentages of Sox2+/Ascl1-tdTomato+ over Ascl1-tdTomato+ cells (control DG: 7.65 $\pm$ 2.62; imaged DG: 9.69 $\pm$ 2.70; $p = 0.616$) and in the percentage of neurons (Sox2-/Ascl1-tdTomato+ over Ascl1-tdTomato+ cells; control DG: 92.34 $\pm$ 2.62; imaged DG: 90.30 $\pm$ 2.70; $p = 0.616$) between control and imaged DG. **(I)** Dot plot showing no difference in the number of recombined neurons and Sox2+ cells per mm^2 in imaged animals and control animals without window and without anesthesia (neurons control: 0.79 $\pm$ 0.049; neurons imaged: 0.69 $\pm$ 0.14; $p = 0.5765$; Sox2+ cells control: 0.06 $\pm$ 0.02; Sox2+ cells imaged: 0.10 $\pm$ 0.005; $p = 0.1736$). Statistical test used: unpaired two-tailed t-test. All values are shown as mean $\pm$ s.e.m. Scale bars represent: 50μm (D), 100μm (B, E, G).

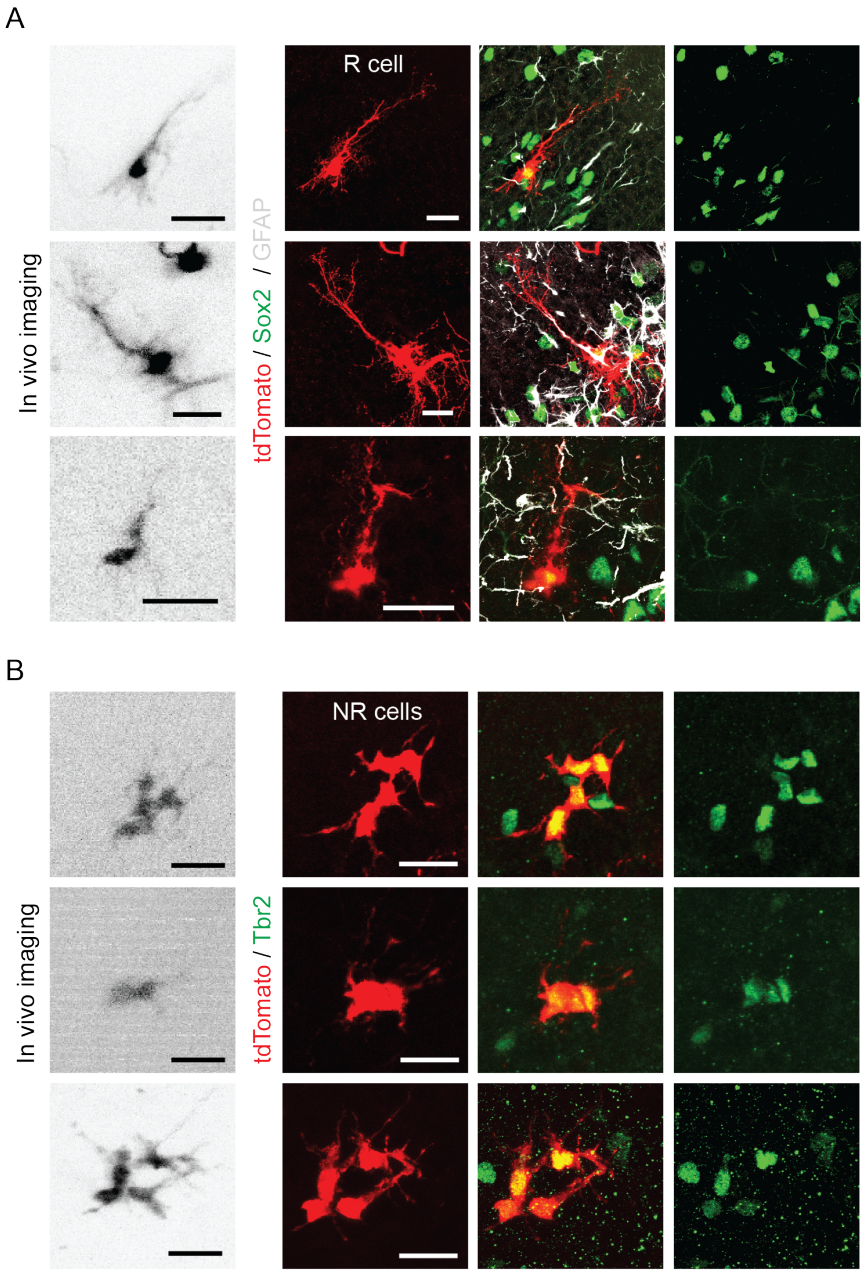

Figure S2: High consistency between marker expression and cell classification based on in vivo imaging. (A) Shown are examples of cells classified as R cells during *in vivo* imaging (left panels). *Post hoc* immunohistochemistry and detailed confocal imaging reveal that Ascl1-labeled tdTomato-expressing R cells (red) co-label with Sox2 (green; 19 of 20 *post hoc* analyzed cells) and also express GFAP. Note that in the second example of R cells, the cell in the upper right corner in the *in vivo* image is not visible in the post hoc immunohistochemistry due to a small shift in the cutting plane. **(B)** Shown are examples of cells classified as NR cells during *in vivo* imaging (left panels). *Post hoc* immunohistochemistry and confocal imaging reveal Ascl1-labeled tdTomato-expressing NR cells (red) co-label with Tbr2 (green; 80 of 90 *post hoc* analyzed cells) showing high consistency between cell classification based on *in vivo* imaging information and *post hoc* molecular marker expression. Scalebars represent 20 μm.

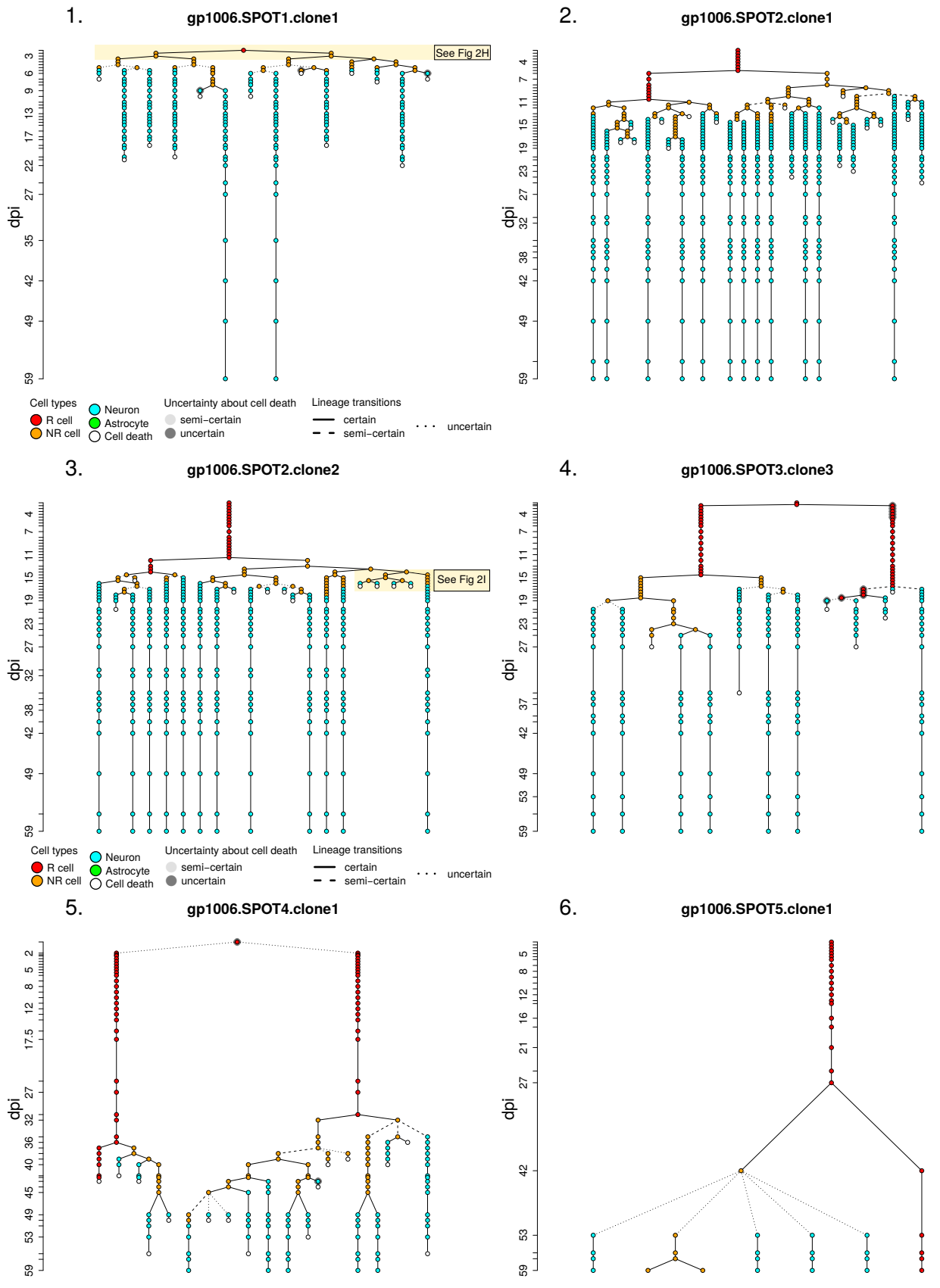
1.
gp1006.SPOT1.clone1
See Fig 2H
dpi
2.
gp1006.SPOT2.clone1
dpi
Cell types
R cell
NR cell
Neuron
Astrocyte
Cell death
Uncertainty about cell death
semi−certain
uncertain
Lineage transitions
certain
semi−certain
uncertain
3.
gp1006.SPOT2.clone2
See Fig 2I
dpi
4.
gp1006.SPOT3.clone3
dpi
Cell types
R cell
NR cell
Neuron
Astrocyte
Cell death
Uncertainty about cell death
semi−certain
uncertain
Lineage transitions
certain
semi−certain
uncertain
5.
gp1006.SPOT4.clone1
dpi
6.
gp1006.SPOT5.clone1
dpi

7. gp1006.SPOT6.clone1

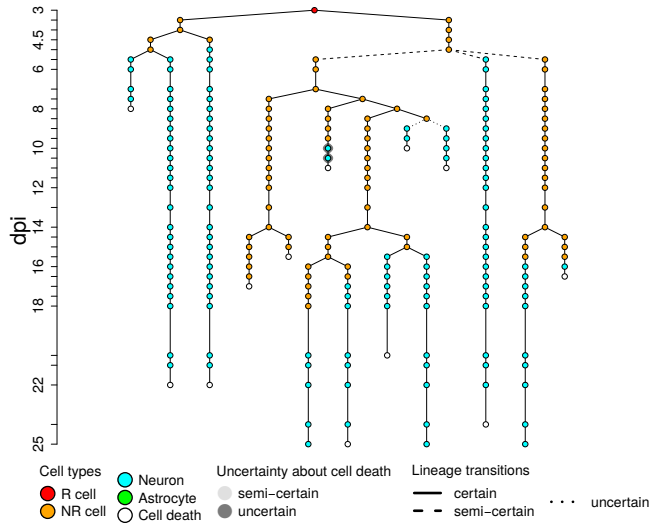

8. gp519.SPOT10.clone1

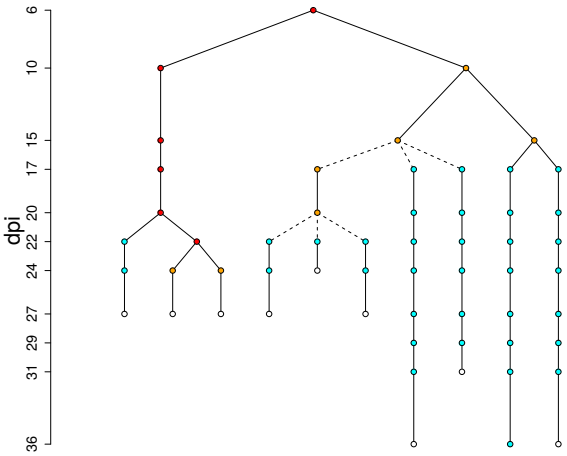

9. gp519.SPOT5.clone1

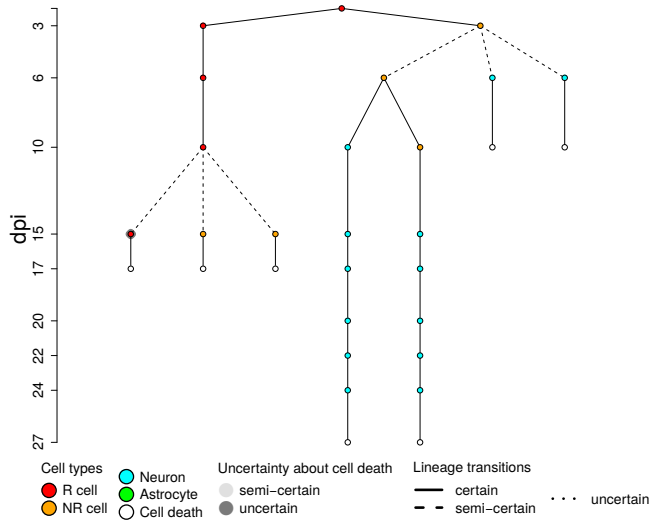

10. gp519.SPOT7.clone1

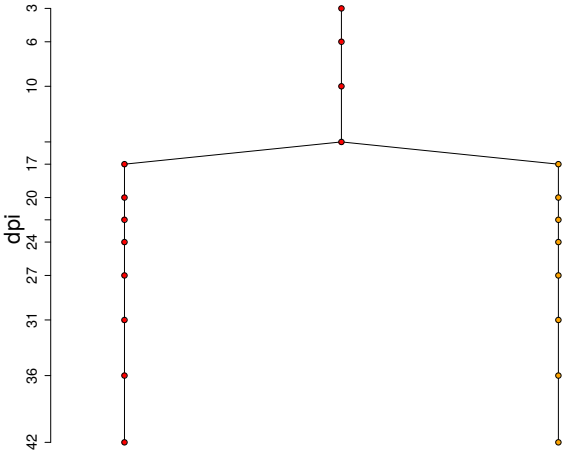

11. gp522.SPOT2.clone1

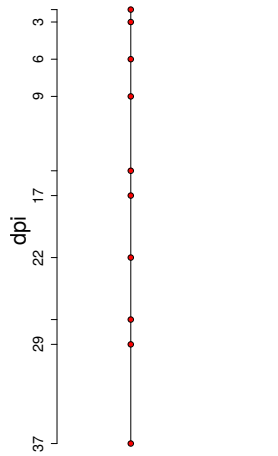

12. gp522.SPOT3.clone1

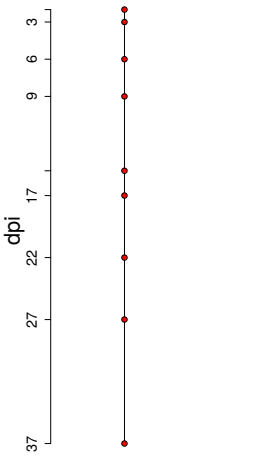

13. **gp522.SPOT4.clone1**

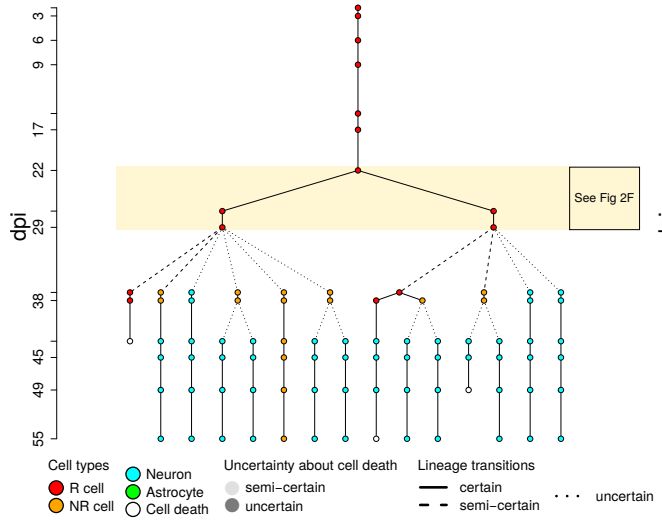

14. **gp522.SPOT4.clone2**

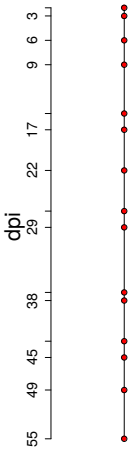

15. **gp522.SPOT7.clone1**

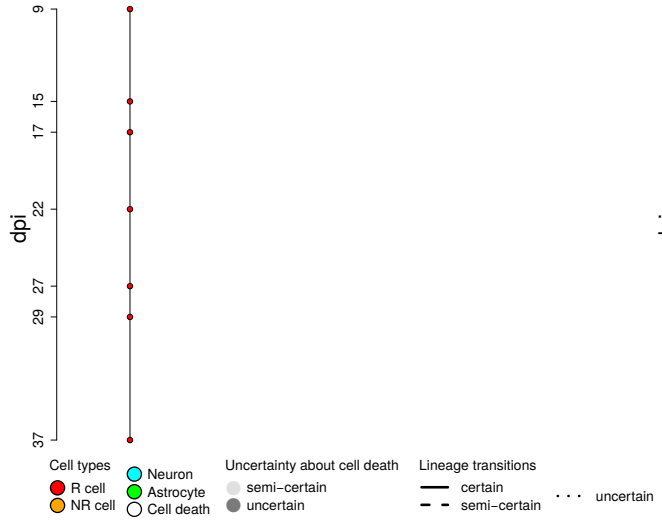

16. **gp522.SPOT7.clone2**

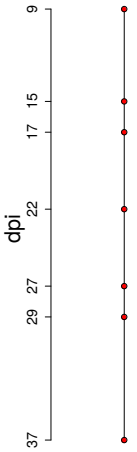

17. **gp611.SPOT1.clone1**

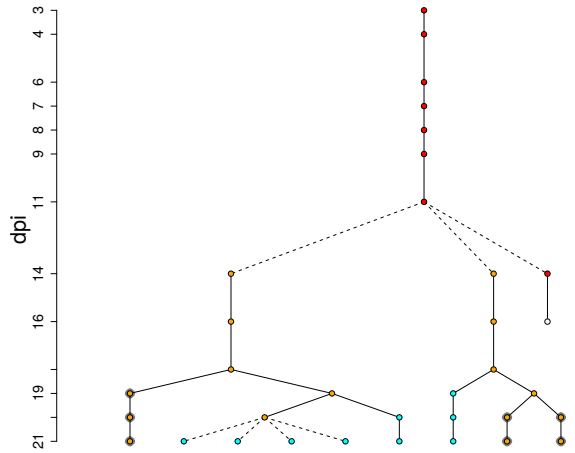

18. **gp611.SPOT1.clone2**

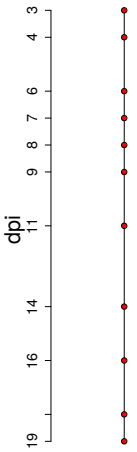

19. **gp611.SPOT1.clone3**

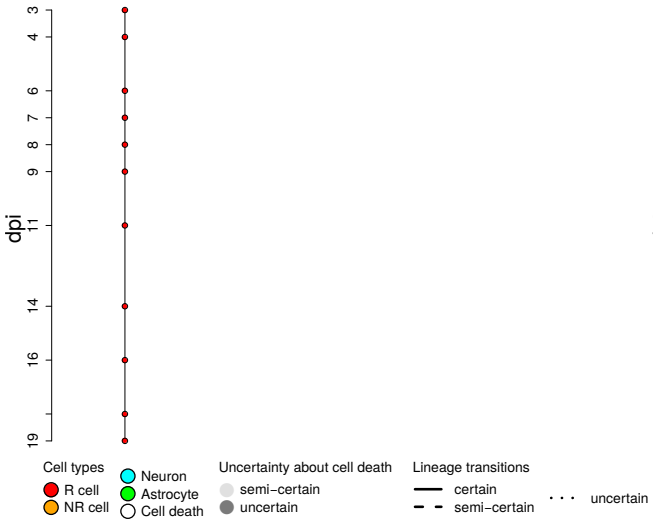

20. **gp672.SPOT1.clone1**

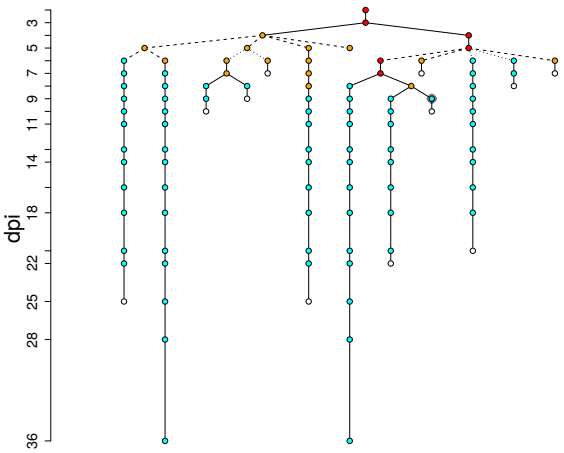

21. **gp672.SPOT1.clone2**

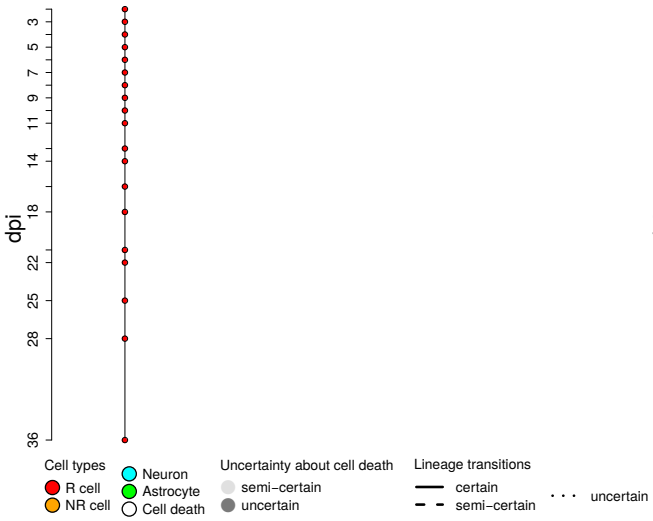

22. **gp672.SPOT1.clone3**

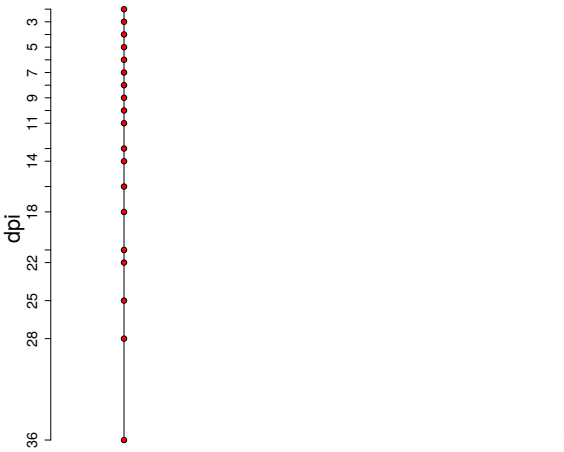

23. **gp672.SPOT3.clone2**

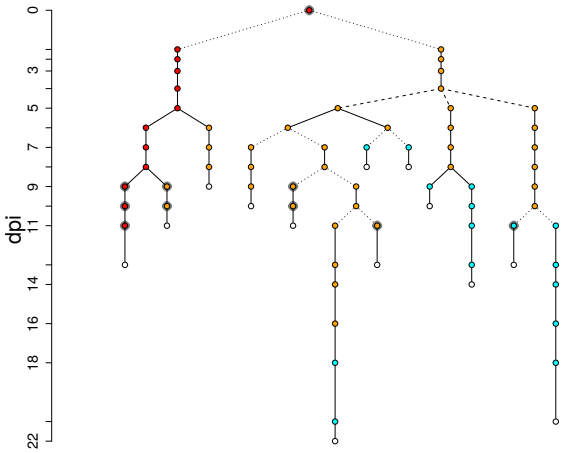

24. **gp672.SPOT3.clone3**

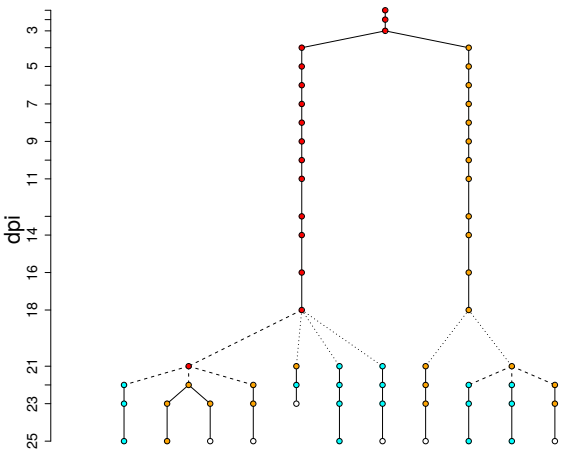

25. gp672.SPOT7.clone1

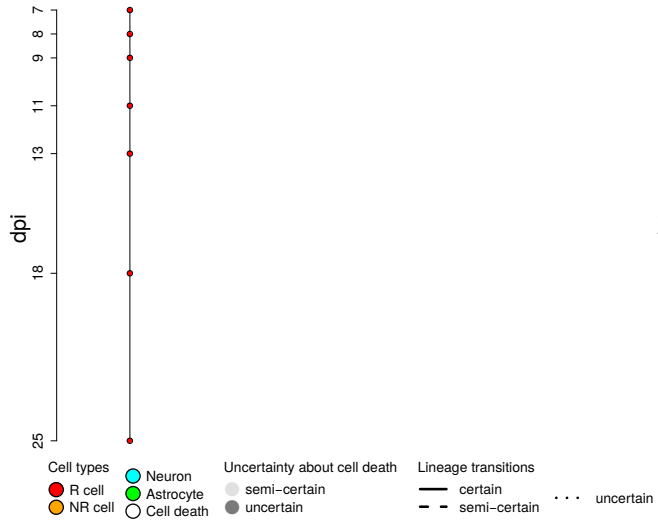

26. gp742.SPOT1.clone1

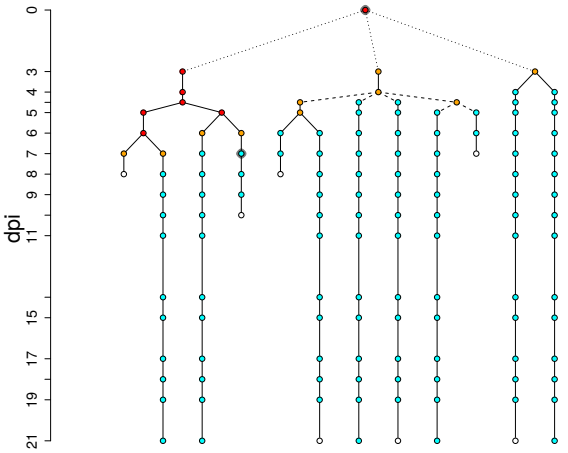

27. gp742.SPOT2−1.clone1

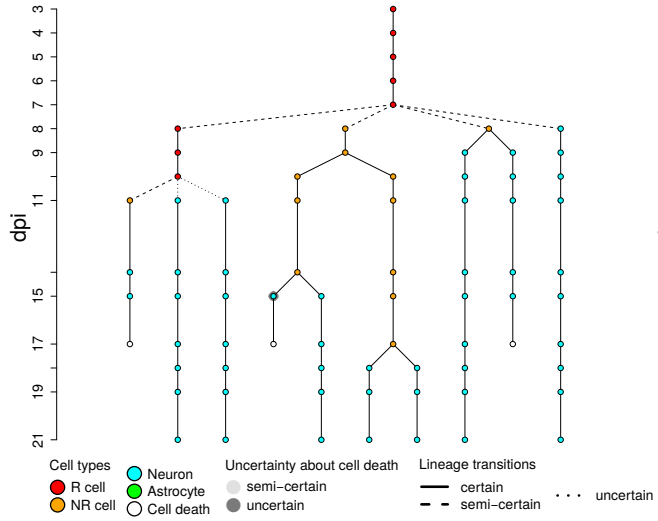

28. gp747.SPOT2.clone1

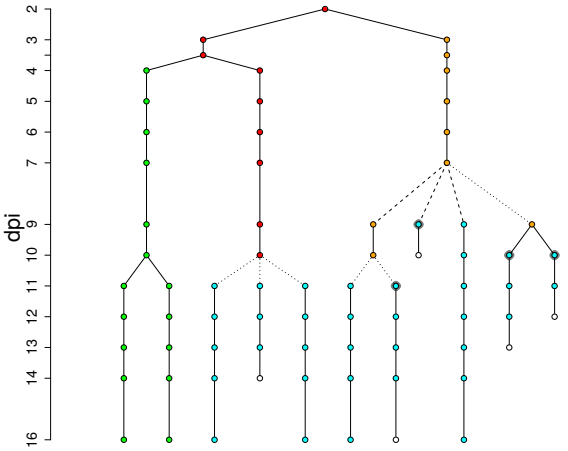

29. gp747.SPOT2.clone2

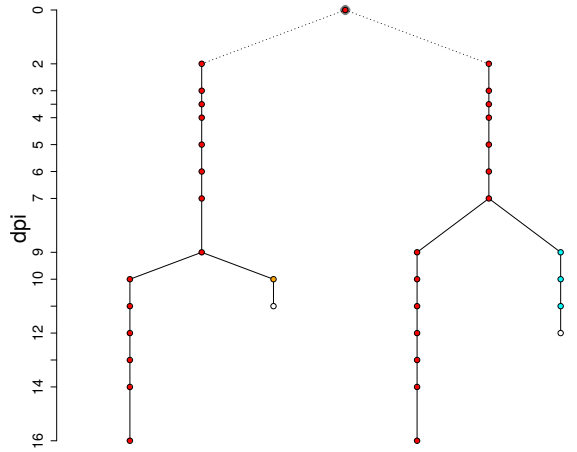

30. gp747.SPOT4.clone1

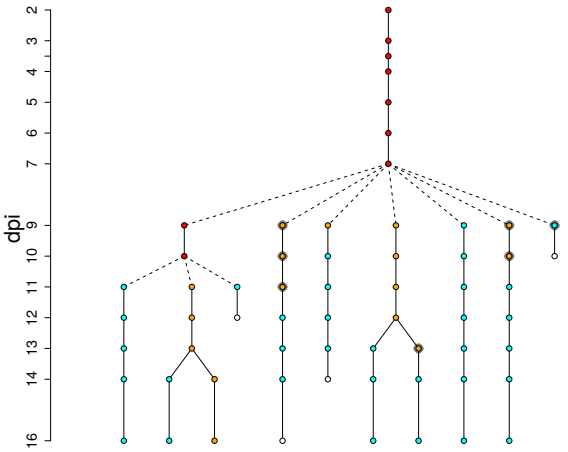

31. **gp808.SPOT11.clone1**

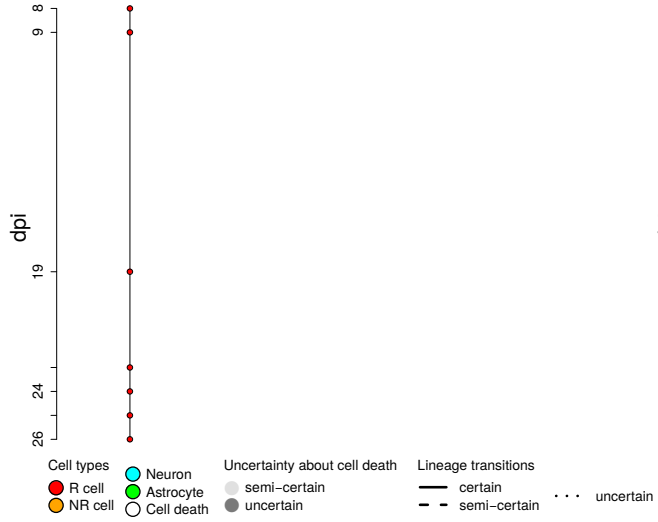

32. **gp808.SPOT11.clone2**

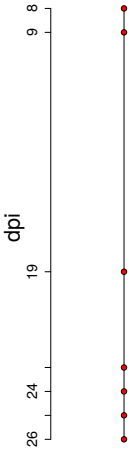

33. **gp808.SPOT12.clone1**

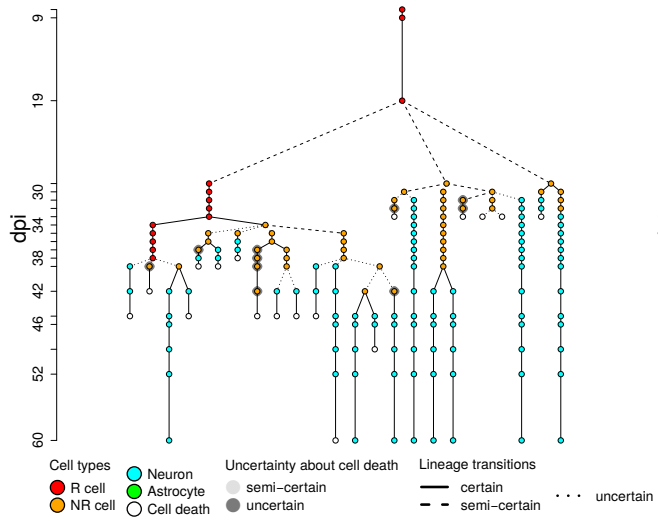

34. **gp808.SPOT12.clone2**

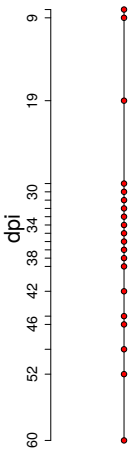

35. **gp808.SPOT13.clone1**

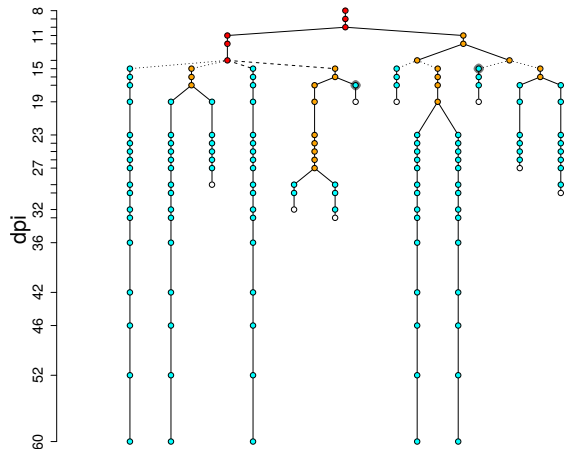

36. **gp808.SPOT2.clone1**

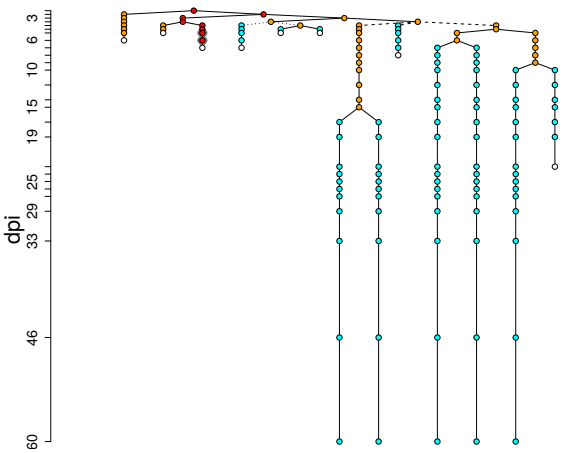

37. **gp808.SPOT20.clone1**

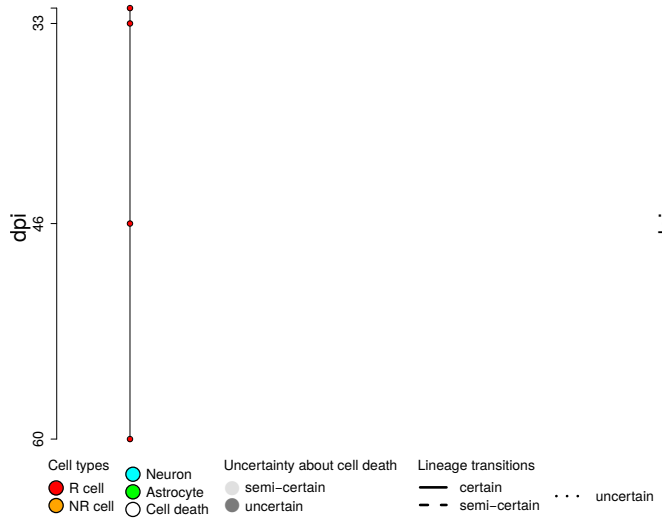

37. **gp808.SPOT21.clone1**

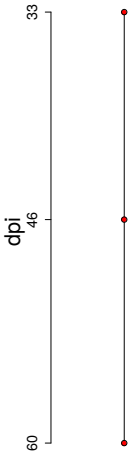

39. **gp808.SPOT5.clone1**

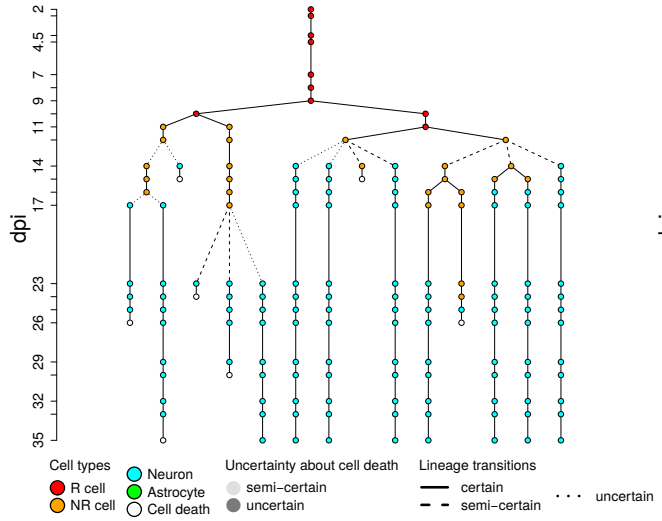

40. **gp818.SPOT1.clone1**

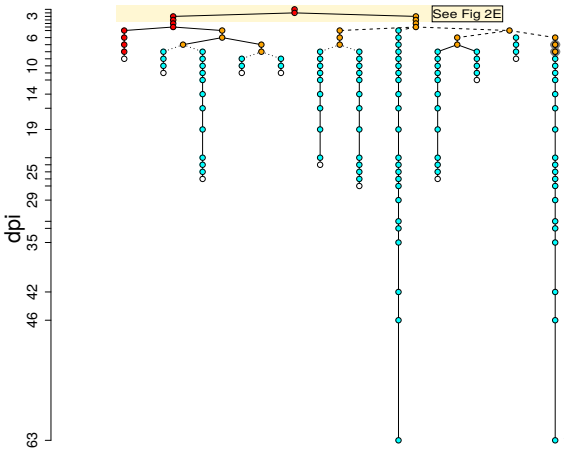

41. **gp818.SPOT10.clone2**

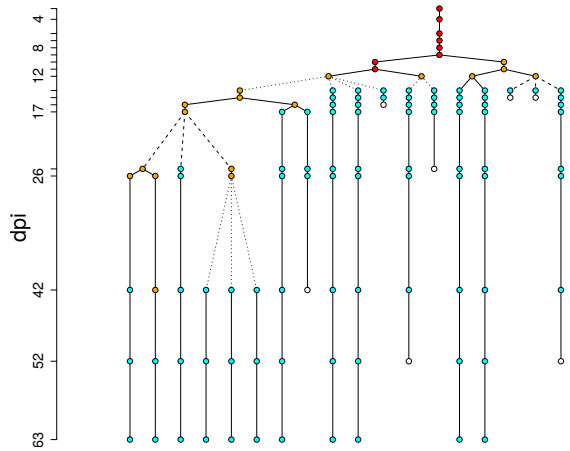

42. **gp818.SPOT14.clone1**

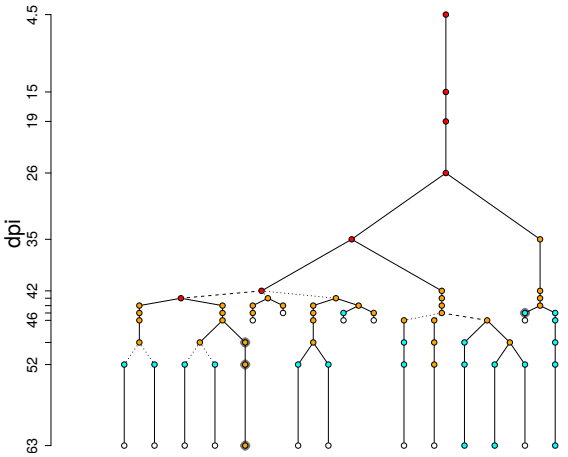

49. gp818.SPOT2.clone2

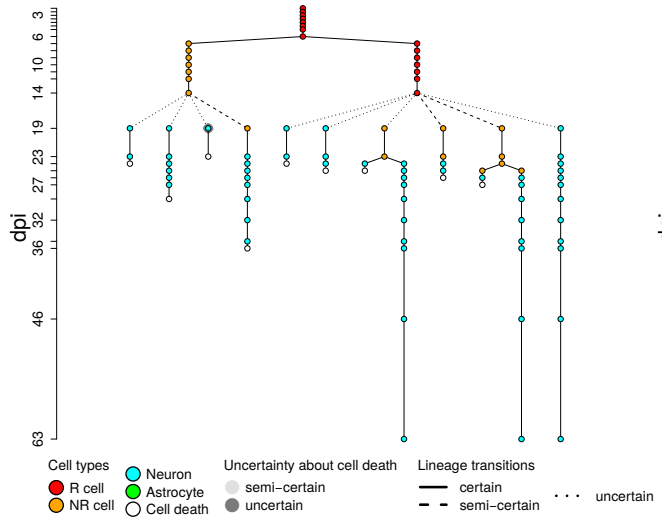

50. gp818.SPOT2.clone3

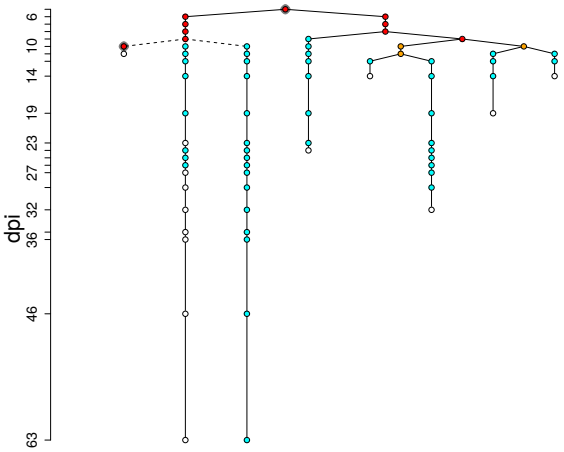

51. gp818.SPOT2.clone4

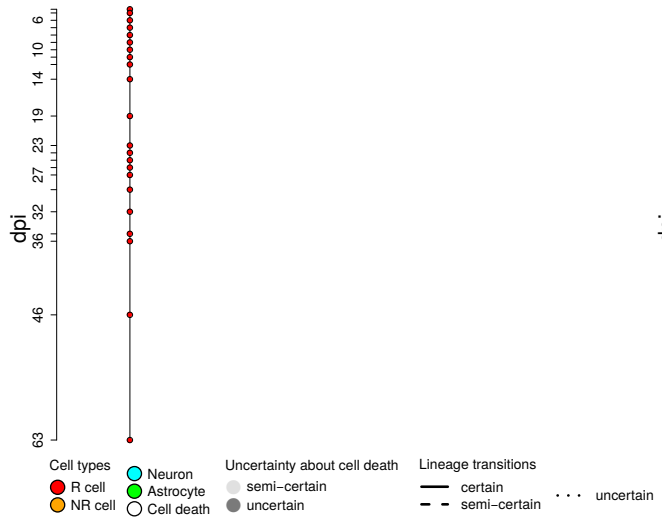

52. gp818.SPOT3.clone1

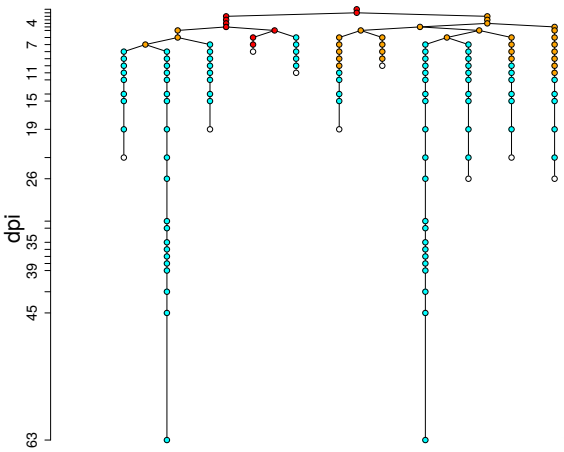

53. gp818.SPOT3.clone2

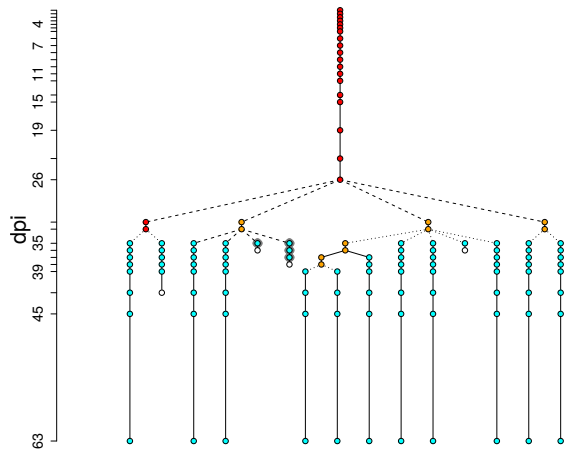

54. gp818.SPOT4.clone1

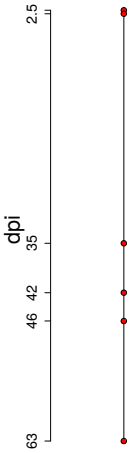

55. **gp818.SPOT5.clone1**

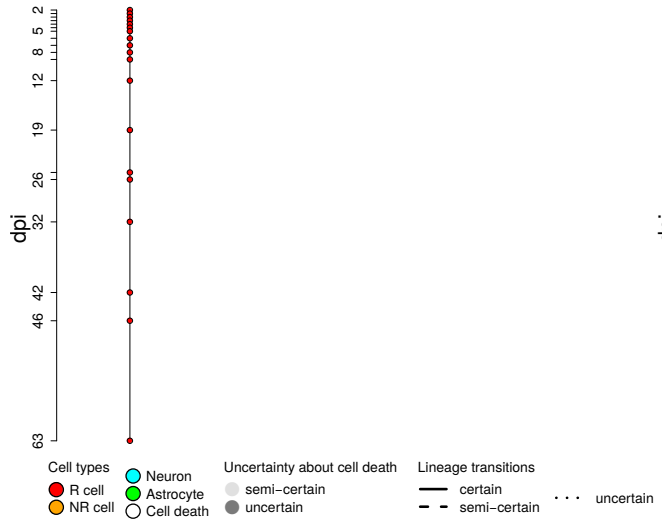

56. **gp818.SPOT6.clone1**

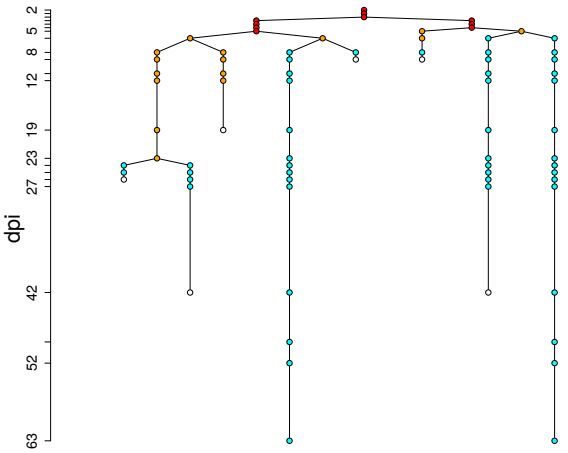

57. **gp818.SPOT6.clone2**

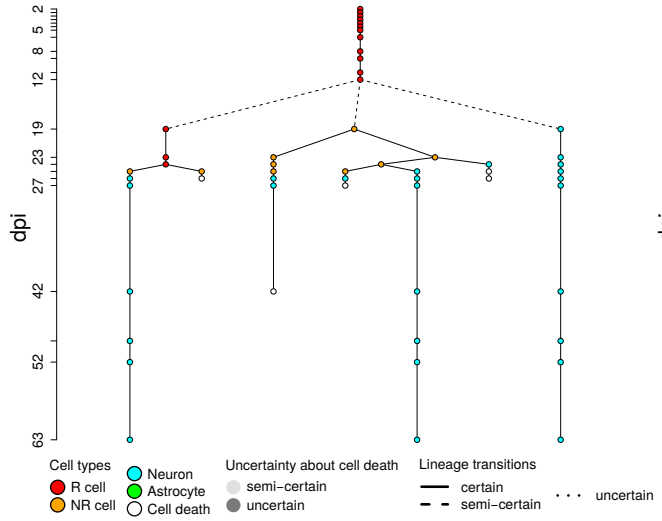

58. **gp818.SPOT6.clone3**

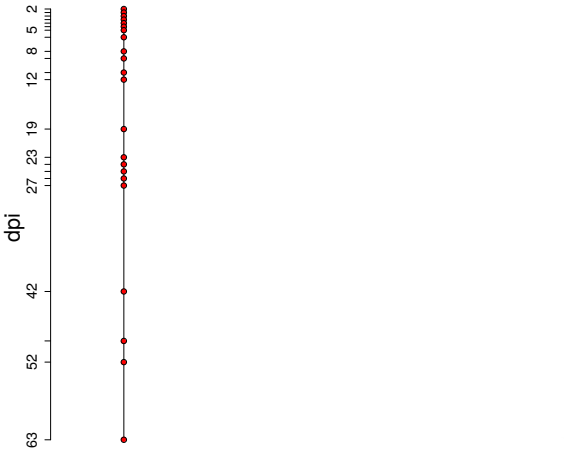

59. **gp818.SPOT6.clone4**

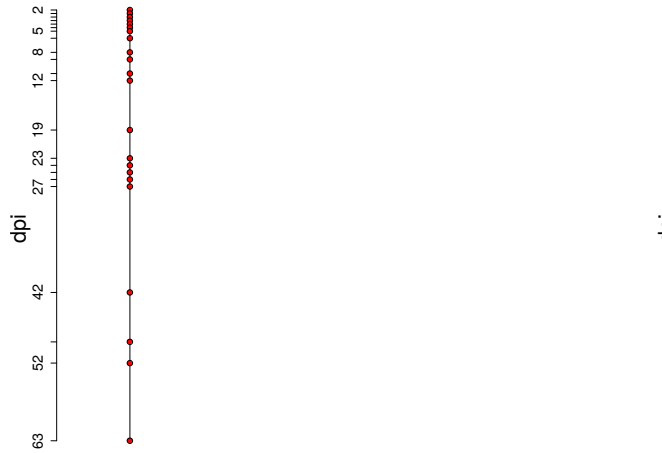

60. **gp818.SPOT7.clone1**

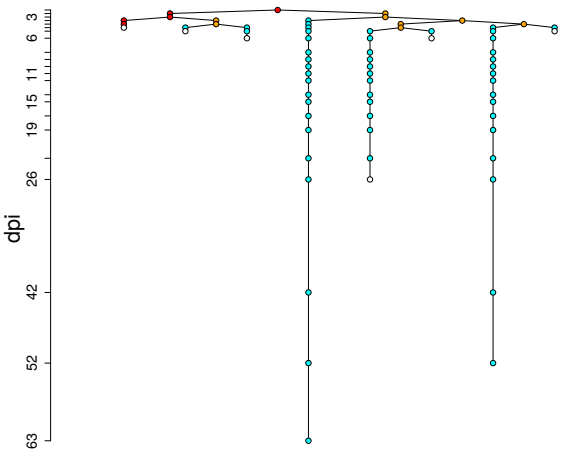

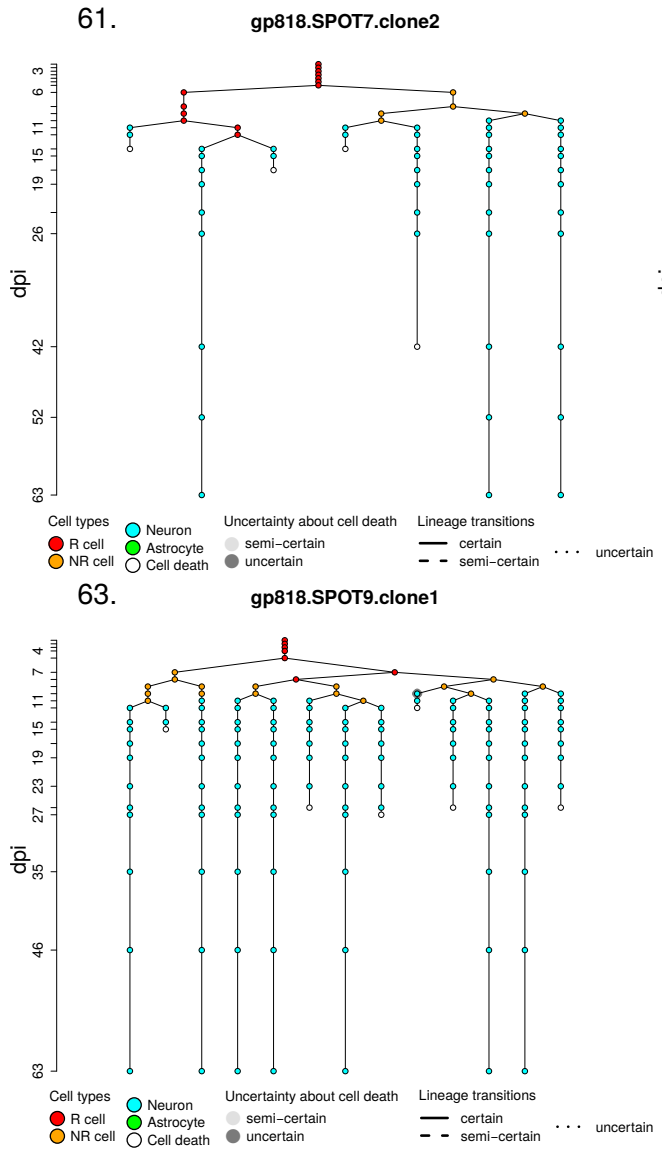

Figure S3: Lineage trees constructed from chronic imaging of Ascl1-tdTomato-labeled NSPCs. Lineage trees obtained from annotation of R lineages ($n = 63$ from 9 experimental mice). The different cell types follow a color-coding that is indicated on each page. Uncertainty concerning the cell type is shown by grey shades around cells. The certainty of lineage transitions is represented by either solid, dashed or dotted lines. The scale on the left (days) indicates the duration of the imaging time. Each cell depicted represents a z-stack taken at an imaging time point. Lineage trees appear in the order of experimental animals they are obtained from (note that an internal nomenclature is used). Parts of lineage trees underlined in yellow correspond to division type examples shown in Figure 2. Note: Lineage trees depicted here are of sufficient resolution allowing for detailed inspection using electronic zoom.

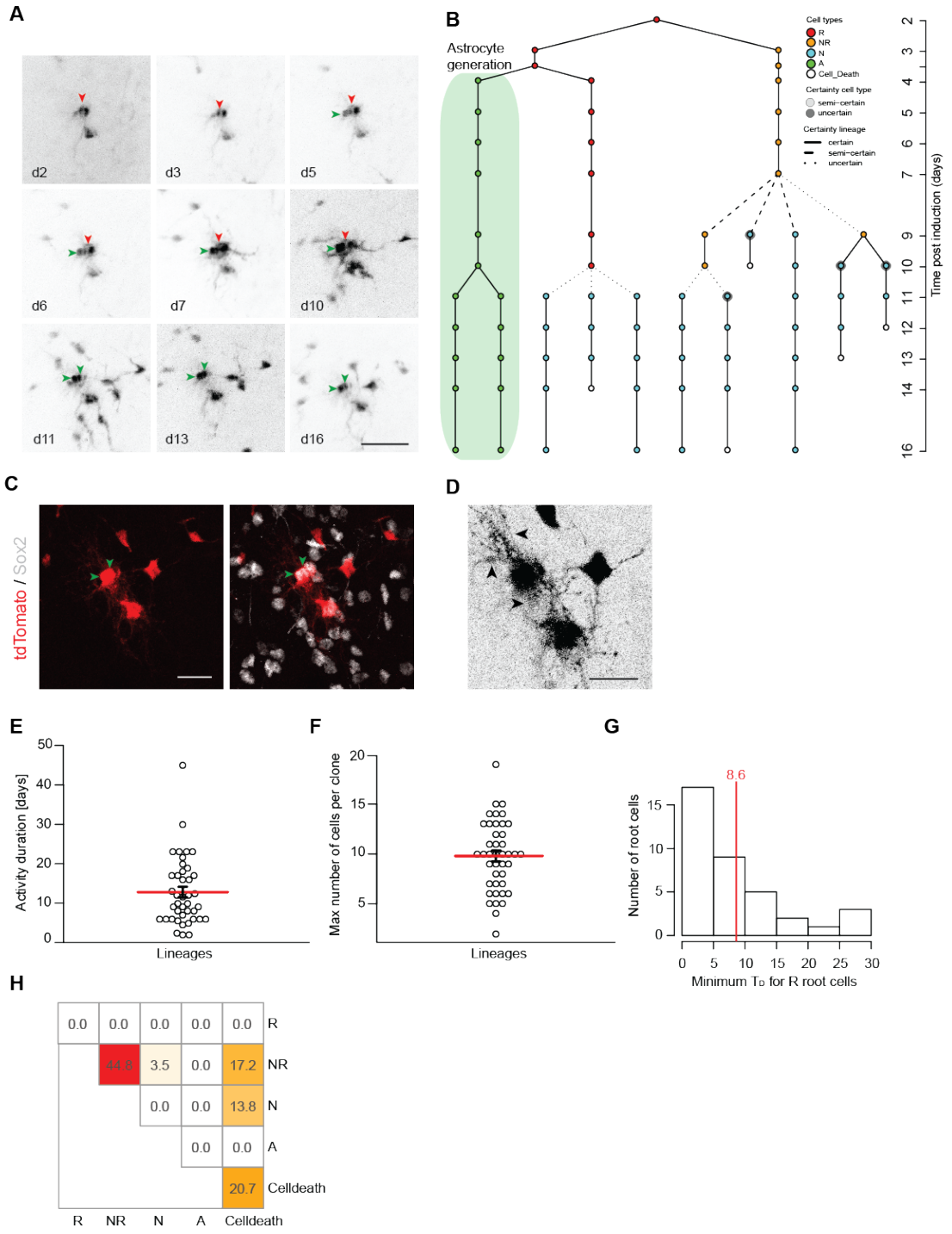

Figure S4: Potency and clonal expansion of individual Ascl1-labeled R cells. (A) Ascl1- labeled cells can generate neuronal and glial progeny. Shown are images (collapsed z-stacks) of selected time points from the observation of an Ascl1-expressing R cell and its progeny. Initial R cell (red arrowhead) and astrocytes (green arrowhead) that were generated by that R cell are indicated. **(B)** Lineage tree deduced from the imaged NSPC clone depicted in A. The appearance of astrocytes is highlighted in green. One out of 42 active R lineages, one generated astrocytic progeny (2.4%). **(C)** Post-imaging immunostaining of the imaged area in A. The two astrocytes are identified as

Sox2 (grey) positive cells with classical astrocytic morphology (green arrowheads). **(D)** Single z-plane from confocal microscopy in C demonstrating the ramified morphology of the two astrocytes (black arrowheads; inverted picture). **(E)** Activity duration measured as the time between the first and last division in each lineage (12.81 $\pm$ 1.35 days; $n = 41$). **(F)** Maximum number of cells generated per lineage (9.79 $\pm$ 0.54; $n = 42$). Note that the final clone size was on average 4.8 $\pm$ 0.55 cells per active R cell clone. **(G)** Time until the first division of R root cells calculated from the start of the imaging 2dpi (8.7 $\pm$ 1.3 days; $n = 36$). **(H)** Heat map depicting the frequencies for the fate of R cells after the depleting division ($n = 29$ divisions). Values are shown as mean $\pm$ s.e.m. Scale bars represent 50μm (A), 20μm (C, D).

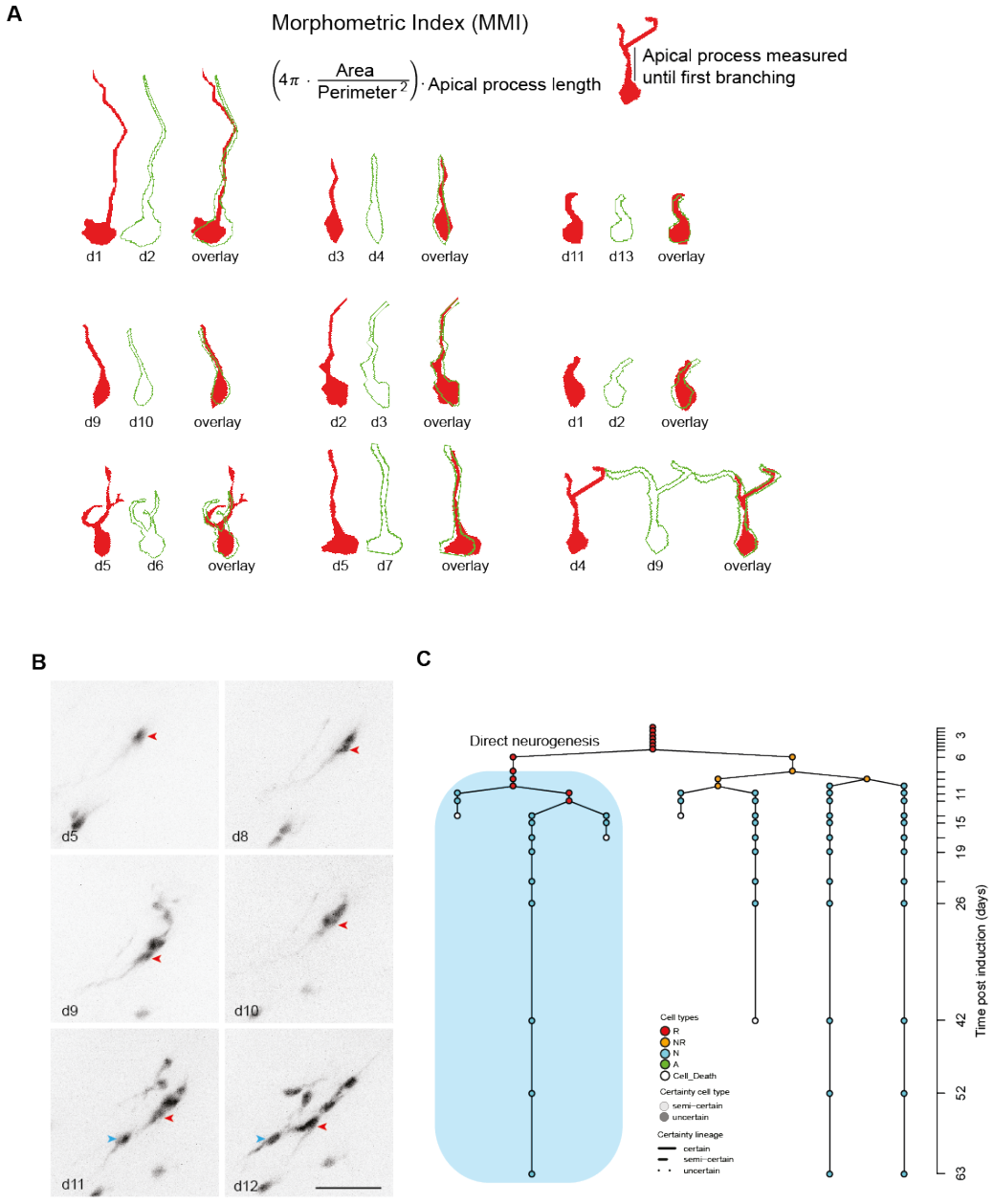

Figure S5. Morphology of R mother cells remains highly stable during asymmetric cell divisions. (A) Outlines of R cells before (red) and after (green) asymmetric cell divisions. An overlay of both states is shown. The Morphometric Index (MMI) is calculated as product of circularity and apical process length (which is measured from edge of the cell body to first branching; see Materials and Methods). Note the high stability of the cell morphology. (e.g. major process length and orientation; $n = 9$). **(B)** Images (collapsed z-stacks) of selected time points from the observation of an R cell showing direct generation of a neuronal cell. Initial R cell (red arrowhead) and directly generated neuron (blue arrowhead) are indicated. **(C)** Lineage tree constructed from the imaged NSPC clone depicted in B. The direct generation of neurons from an R cell is highlighted in blue. Scale bar represents 50µm.

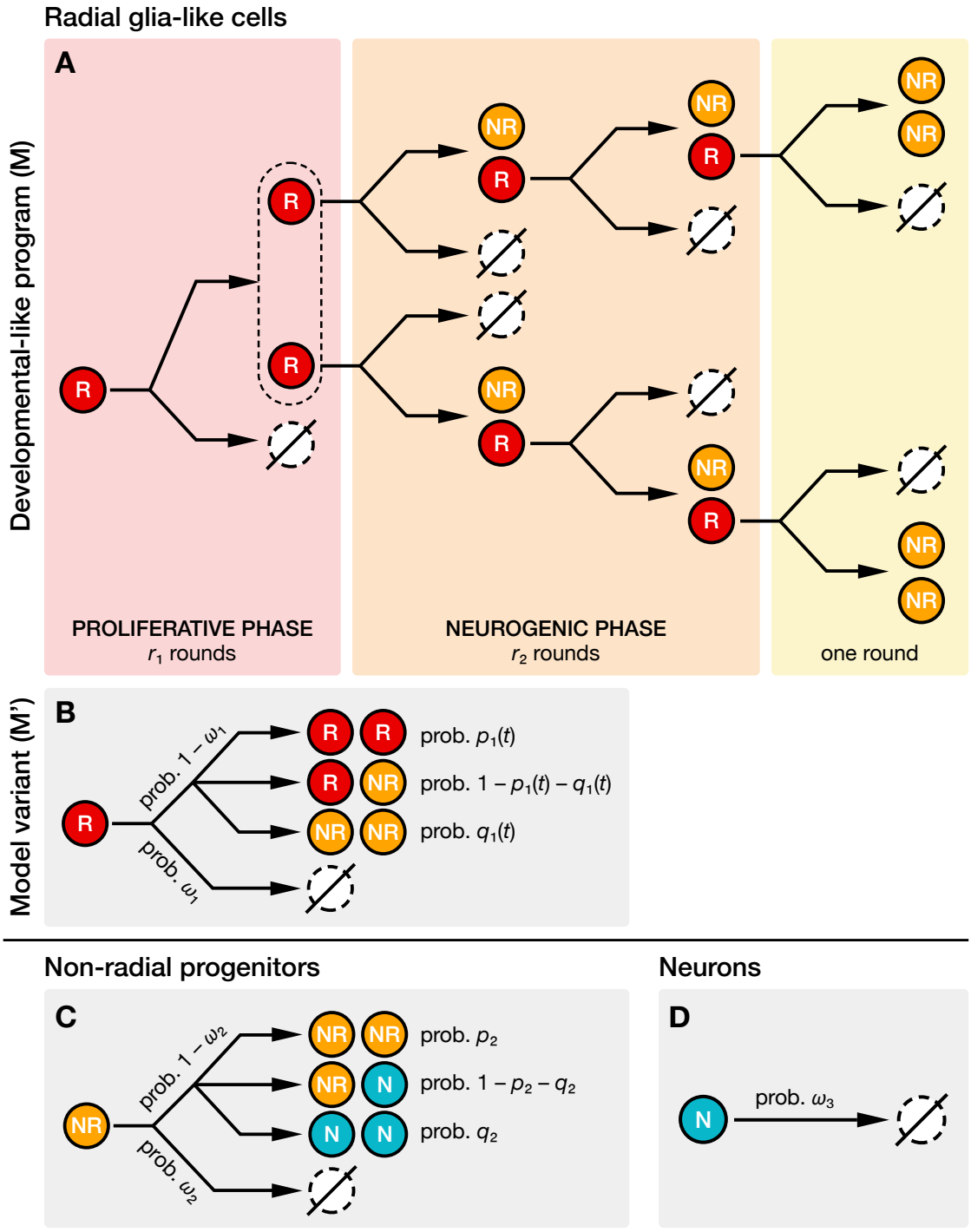

Figure S6. Schematic depiction of the cell fate rules of the theoretical model. **(A)** Cell fate rules for R cells following a developmental-like program. **(B)** Model alteration with stochastic rules for R cells with time-dependent fate probabilities. **(C)** Completely stochastic cell fate choices for non-radial progenitors. **(D)** Neurons stochastically undergo cell death.

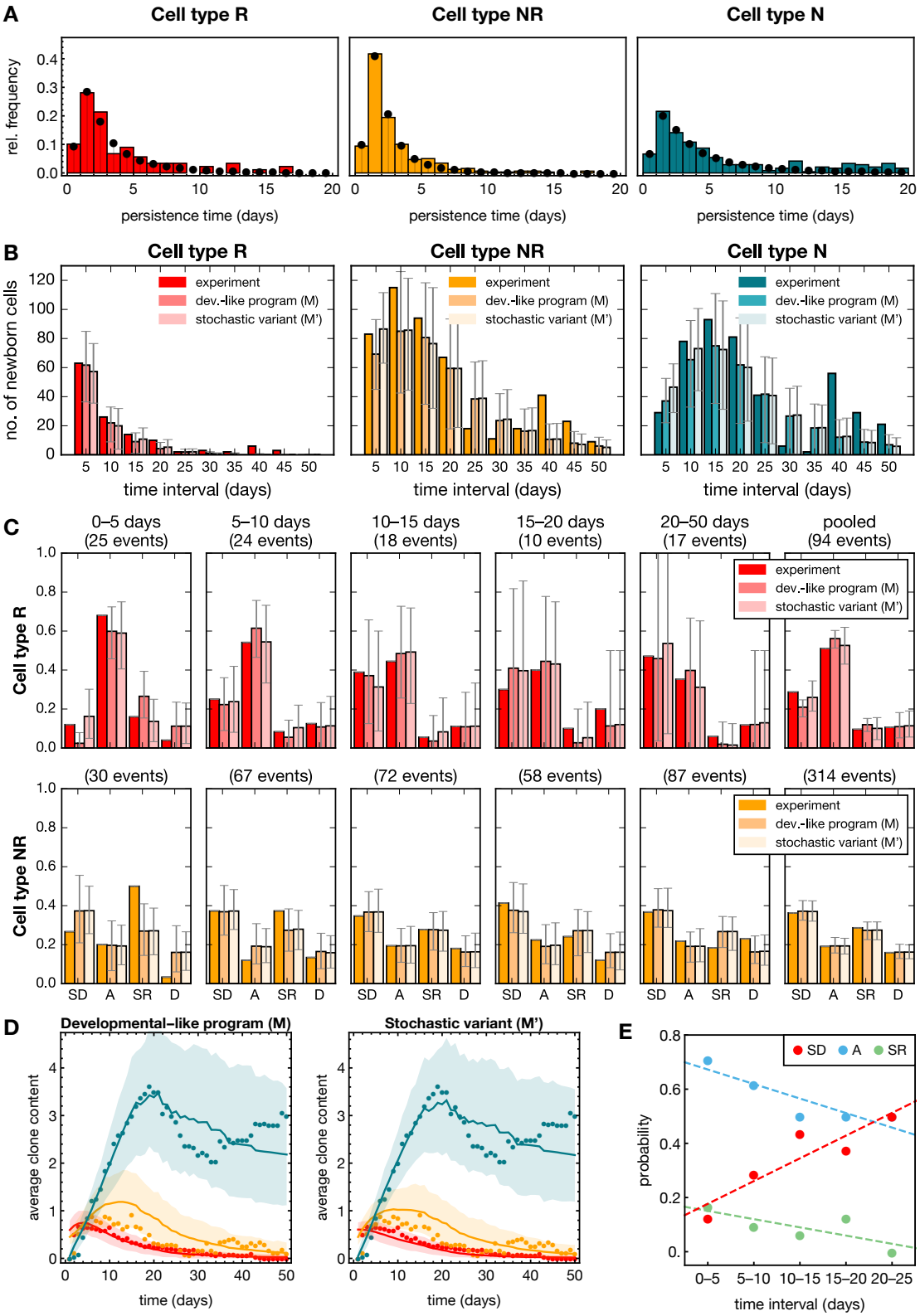

Figure S7. Comparison of model simulations and experiment. **(A)** Persistence time distributions obtained from experimental lineage trees (colored bars) along with the best fit by the discrete Fréchet-type distribution Eq. (S1) (black dots) for different cell types. The best fit parameters are

given in Supplementary Table S2. **(B)** Number of cells born in successive time intervals. Plots show the total number $m_{x,k}$ of cells of cell type $x = \mathrm{R}, \mathrm{NR}, \mathrm{N}$ that are born within the time interval with index k from experiment and from model simulations. **(C)** Cell fate distributions in successive time intervals. Plots show the relative frequencies $P_{x,\eta,k}$ of cell fate $\eta = \mathrm{SD}, \mathrm{A}, \mathrm{SR}, \mathrm{D}$ for cell type x and time interval with index k from experiment and model simulations of the the developmental-like program and the stochastic variant. Bars show the relative frequencies of symmetric differentiation divisions (SD), asymmetric divisions (A), symmetric self-renewing divisions (SR), and cell death (D). Early time intervals are 5 days, late time intervals (20–50 days) with small numbers of events have been pooled together. Conventions as in panel C. **(D)** Average clonal content (number of cells) of different cell types as a function of time from experiments (dots) and simulations (lines) of different model variants as indicated. In panels B–D, simulation results indicate averages over 500 realizations of all considered lineage trees as described in the Supplementary Text. Error bars and shaded areas indicate the regions in which 95 % of the simulation results fall. Simulation parameters are given in Supplementary Table S2. **(E)** Time-dependent cell fate frequencies for radial-glia like cells as determined from experiments (dots) and fits (dashed lines) of the linear functions $p_1(t) = c_p - \kappa_p t$ for the SR dataset (red), $q_1(t) = c_q + \kappa_q t$ for the SD dataset (orange) and the resulting function $1 - p_1(t) - q_1(t)$ for the A dataset (green). The corresponding fit parameters c_p, c_q, κ_p, and κ_q are reported in Supplementary Table S2.

3 Supplementary Tables

Param.	Value	Description
Cell ID	unique identifier (ID)	corresponds to the generation in the lineage it is born (first digit) and the prospective sequence in the lineage it appears (second digit).
CellType	1	**R cells**: Cell with one longer primary process, often ending with a branched tuft. Also smaller processes at the cell soma and primary process (distinguishing from neurons). Stable in position and morphology during quiescence and after asymmetric divisions. Identified in post imaging immunostaining as Sox2 and GFAP positive and Tbr2 negative.
	2	**NR cells**: No stable long primary process (unlike R). Round or trapezoid-shaped morphology with few shorter processes. Morphology changing rapidly. Identified in post imaging immunostaining as Tbr2 positive and GFAP negative.
	3 and 4	Young and mature **neurons** respectively. Non-dividing cells. Small cell body with a clear leading process that is often rapidly changing orientation. Rapid movement during first 14 days after birth (young neurons). Immobile cell displaying a big drop-shaped and smooth cell body with dendritic arbors (mature neurons). Identified in post imaging immunostaining as DCX for the immature neurons, and Prox1 positive / DCX negative for mature neurons.
	5	**Astrocyte**: Numerous small ramified processes all around the cell body. Absence of a single clearly distinguishable longer process.
Uncertainty Type	1	certain cell type: cell fulfills all (or the vast majority) of criteria mentioned above.
	0.5	if one is semi certain about the cell type: indications from morphology, behavior, history speak for one cell type, but some criteria are missing.
	0	the judgment is uncertain: no clear indications from morphology, behavior, history; however the cell is assigned to the most likely cell type annotated with uncertainty 0.
TimePoint		number of the imaging timeframe in which the cell has been annotated.

Param.	Value	Description
MotherID	unique ID	ID of the mother of the current cell. Usually located in the neighborhood of daughter cells at the previous timepoint. Noted as Not Available (NA) if the cell is the first cell of a clone.
Uncertainty Mother	1	mother cell is certain: location and morphology are clearly identifying the mother cell in the previous timepoint; only possible when exactly 2 clear daughter cells
	0.5	lineage transition is semi-certain: some indications from location and morphology, but some criteria are missing for example if more than 2 cells could be daughter cells
	0	uncertain: impossible to determine the mother cell, because several potential mothers are close or because ambiguous relative cell location; then the most probable annotation is chosen with label 0, uncertain.
SisterID	unique ID	Cell ID of the prospective second daughter cell that originates from a common mother cell. Features like location of cells in relation to all surrounding cells. The second digit in the cell ID is added in a continuous fashion.
Uncertainty Sister	1	certain about the common mother cell (sister relationship) common features concerning morphology and location
	0	uncertain about sister relationship: not all parameters regarding morphology, location and behavior support the relationship
CellDeath	0 added to the code	Cell disappears from its previous location (without movement to another location), or apoptotic bodies at this location appear.

Table S1 Parameter list describing how each cell is coded in the clones.

Param.	Value	Description	M	M'
		R cells		
μ_{R}	1.29	parameters of the persistence time distribution	•	•
ν_{R}	1.94			
ω_{R}	11 %	probability of cell death	•	•
r_1	1	rounds of SR divisions	•	
r_2	2	rounds of A divisions	•	
c_p	17 %	initial probability for SR divisions		•
c_q	13 %	initial probability for SD divisions		•
κ_p	0.61 % d^{-1}	probability change rate for SR division		•
κ_q	1.68 % d^{-1}	probability change rate for SD divisions		•
		NR cells		
μ_{NR}	1.78	parameters of the persistence time distribution	•	•
ν_{NR}	1.59			
ω_{NR}	16 %	probability of cell death	•	•
p_{NR}	33 %	probability for a symmetric self-renewing division	•	•
q_{NR}	44 %	probability for a symmetric differentiating division	•	•
		N cells		
μ_{N}	1.04	parameters of the persistence time distribution	•	•
ν_{N}	2.55			
ω_{N}	39 %	probability of cell death	•	
	35 %			•
		Global simulation parameters		
G	4	uncertainty in the initial generation	•	
	2			•

Table S2 Parameter list and best fit parameters for the theoretical model. The columns M and M' indicate to which model variant the respective parameter applies.

4 Supplementary Movies

Movie S1. Example analyses of *in vivo* imaged R cells. Shown are examples of 3 individual R cells obtained during *in vivo* imaging sessions. Shown are in order: all single z-planes that contain information on the individual R cell repeated twice (sequence is indicated at the bottom left; z-stepsize is 5μm), the maximum projection of all z-planes, and a rotating 3D reconstruction of the R cell to illustrate the overall morphology of imaged R cells, including the extension of a typical long basal process.

Movie S2. Illustration of image-based cell annotation. This movie illustrates the annotation of cell types using the information of all z-planes during all imaging time points. Shown is a clonal lineage starting with an R cell at 2dpi followed until 63dpi (corresponding to lineage 40 in Figure S3). For four time points in the lineage (d2.5, d3, d6 and d12), sequences of all single z-planes are shown in addition to the maximum projections, to illustrate that the cell type judgement is based on detailed inspection of cell morphology through all z-planes. After each scan through a z-stack, color-coding on the maximum projection illustrates the annotated cell types (R cell: red, NR cell: orange, Neuron: blue). Cells not belonging to the clone are not annotated. Note the asymmetric division of the R cell (d2.5 to d3; NR cell generated) and the persistence of the R cell until d8 (visible basal process of the R cell remains; see z stack at d6). Small shifts in x and y at different time points have been corrected.

Movie S3. Chronic in vivo imaging of two individual R cells. Shown is the lineage progression of two initial R cells that get activated at distinct time points and generate neuronal progeny (corresponding to Figure 1D, E and lineages 2 and 3 in Figure S3). Note the occurrence of cell death, cell migration and maturation of granule cells during the time course. Small shifts in x and y at different time points have been corrected.